

# Libron-phonon coupling effect on the infrared absorption spectra of molecules trapped in matrices

I. L. Garzón

*Instituto de Física, Universidad Nacional Autónoma de México, Apdo. Postal 20-364, 01000 México, D.F., México*

Estela Blaisten-Barojas

*Department of Chemistry, Stanford University, Stanford, California 94305 and Instituto de Física, Universidad Nacional Autónoma de México, Apdo. Postal 20-364, 01000 México, D.F., México*

(Received 25 February 1985; accepted 22 July 1985)

The libron-phonon coupling (LPC) model is used to calculate the IR absorption coefficient of diatomic molecules trapped in solid matrices at low temperatures. The coupling between the collective motions of the crystal and the molecule libration-type motion is at the basis of the LPC model. This coupling results in temperature dependent shifts and broadening of the spectral lines even in the low temperature regime. The near IR experimental spectra of CO in Ne, Ar, Kr, and Xe matrices are successfully interpreted with the present theory. The strength of the libron-phonon coupling and other constants pertaining to the theory are reported. The far IR spectra is predicted as well.

## I. INTRODUCTION

The interaction between diatomic molecules and solid matrices has been studied theoretically by means of static and dynamic models. This interaction is of fundamental interest since it modifies the molecular spectroscopic properties with respect to the gas phase. In fact, at low temperatures the monomeric absorption spectra consist of a sharp line with shoulders toward higher and lower frequencies.<sup>1</sup> This band profile has been interpreted as the result of a highly hindered rotational motion, or libration, coupled to the crystal collective motions.<sup>2</sup> The purpose of this work is to present a 3D microscopic approach for the calculation of the IR line shape, shifts and widths of nonspherical diatomics trapped in rare-gas matrices. Pauling<sup>3</sup> and Devonshire<sup>4</sup> first discussed this problem by trapping a molecule in a static crystal field. In 1980 Manz<sup>5</sup> generalized these works taking into account the lattice distortion due to the guest molecule. However, static calculations are unable to predict the IR absorption linewidths as well as their temperature dependence.

Dynamical approaches started with the rotation-translation coupling (RTC) model of Friedmann and Kimel,<sup>6,7</sup> later on extended by Mannheim and Friedmann.<sup>8</sup> This treatment does not describe the spectra when molecules with high moment of inertia are present in the matrix. Further progress was provided by Nitzan *et al.*<sup>9</sup> with a multiphonon approach to describe vibrational relaxation. The coupling of phonons to the molecular libration and to the internal vibration was previously studied by one of us<sup>2,10</sup> within a one-dimensional model. The molecule executes a libration-type motion when the crystalline environment produces a high enough potential barrier to the otherwise free rotation.

The results of this approach show that a direct coupling between the molecular internal vibration and phonons is a weak effect that cannot be responsible for the shift and broadening of the  $\nu = 0 \rightarrow \nu = 1$  band.<sup>10</sup> On the other hand, the libron-phonon coupling (LPC) theory lead to temperature dependent shifts and broadenings of the vibration-libration bands as well as of the pure libration spectrum.<sup>2</sup>

More recently, the 2D model of Mauricio *et al.*,<sup>11</sup> in which the molecule is coupled to a viscous isothermal bath via a cage of surrounding atoms, has been compared to Dubost's<sup>1</sup> experimental results with qualitative agreement. For HCl in argon matrices, Allavena *et al.*<sup>12</sup> interpreted the temperature dependent broadening on the basis of phonon-rotational relaxation processes. This approach is adequate whenever the matrix weakly perturbs the molecular rotation.

In this paper we propose that the molecular libration dressed by their interactions with the matrix produces shifts and broadening of the vibration-libration absorption lines. The LPC theory predicts the temperature dependent broadening of CO in rare-gas matrices, successfully reproducing the relevant features of Dubost *et al.* experiments.<sup>1,13</sup> The approach parallels our earlier treatment developed for the IR absorption study of polar diatomics in simple liquid solutions.<sup>14</sup> In Sec. II we describe the system by a model Hamiltonian. Based on linear response theory and a proper connected diagram analysis<sup>15,16</sup> we calculate the Green function associated to the absorption coefficient. In Sec. III we compare our analytical results to CO in rare-gas matrices experiments<sup>1,13,17</sup> and conclude with a discussion.

## II. MODEL AND ABSORPTION COEFFICIENT

The system of interest is a monoatomic matrix with low concentration of diatomic molecules placed as substitutional impurities. We assume that the lattice atoms generate a potential that strongly perturbs the molecular rotation yielding a libration-type motion. Therefore, the molecule is constrained to small angular displacements  $\Delta x$ ,  $\Delta y$ ,  $\Delta z$  (or librations) instead of rotating in its site. Let us describe the molecule at equilibrium in  $S_r$  system fixed in the molecule with  $z$  axis along the molecular internuclear radius  $r$  and with the origin anchored on the molecular center of mass (Fig. 1). The libration is such that angular displacements between  $r$  and  $z$  are small allowing to approximate  $\Delta z$  by  $\Delta r$  and  $p_z$  by zero. Thus, the molecular Hamiltonian is



$$M_\eta = m_\eta^+ a_\eta^+ + m_\eta^{++} a_\eta^+ a_r^+ + m_\eta^- a_\eta a_r^+ + \text{c.c.} \quad (10)$$

Here  $\eta = x, y, z$  and the  $m$  constants are defined in the Appendix.

When an external and oscillating electric field of frequency  $\omega$  and amplitude  $E_0$  is applied to the system molecule-crystal, the absorption coefficient is calculated from the relationship<sup>2,10</sup>

$$\alpha(\omega) = -\Lambda\omega \sum_{\eta=x,y,r} G_\omega''(M_\eta, M_\eta), \quad (11)$$

where  $\Lambda = E_0^2/3V$  in a volume  $V$ . The Fourier transform of the dipole moment-dipole moment Green function is  $G_\omega(M_\eta, M_\eta) = G_\omega' + iG_\omega''$ . It is the latter imaginary part that enters in the above equation. We further use Eq. (10) in Eq. (11) and split the absorption coefficient into a sum of four contributions generated by the various nonvanishing combinations of  $M_\eta$  terms in  $G_\omega''$ <sup>14</sup>:

$$\alpha(\omega) = \alpha_F^-(\omega) + \alpha_N^-(\omega) + \alpha^{+-}(\omega) + \alpha^{--}(\omega). \quad (12)$$

Each component is associated to a Green's function:

$$\alpha^-(\omega) = -\Lambda\omega \sum_{\eta=x,y,r} |m_\eta^+|^2 G_\omega''(a_\eta^+, a_\eta^+),$$

$$\alpha^{+-}(\omega) = -\Lambda\omega \sum_{\eta=x,y} |m_\eta^-|^2 G_\omega''(a_\eta a_r^+, a_\eta a_r^+), \quad (13)$$

$$\alpha^{++}(\omega) = -\Lambda\omega \sum_{\eta=x,y} |m_\eta^{++}|^2 G_\omega''(a_\eta^+ a_r^+, a_\eta^+ a_r^+).$$

In Eq. (12),  $\alpha_F^-(\omega)$  stands for the far IR contribution to  $\alpha^-(\omega)$  given by the sum of terms  $\eta = x, y$  in the first of Eqs. (13), whereas  $\alpha_N^-(\omega)$  stands for the near IR contribution and is given by the  $\eta = r$  term.

We solve the  $G_\omega$  of Eq. (13) in the linear response frame and use a proper connected diagram analysis.<sup>15</sup> Following closely the procedure described in Refs. 14 and 16 up to second order, we obtain

$$\alpha_F^-(\omega) = 2\Lambda\mu_0^2 \left(\frac{x_0}{r_e}\right)^2 \sum_{n_1}^{n_{\max}} \frac{n_{1x} e^{-\beta\epsilon_{n_1}} (1 - e^{\beta\hbar\omega_x}) \omega \Gamma_\omega(n_1)}{[\omega_x + \Delta_\omega(n_1) - \omega]^2 + \Gamma_\omega^2(n_1)}, \quad (14)$$

$$\alpha_N^-(\omega) = \Lambda\mu_1^2 r_0^2 \sum_{n_1}^{n_{\max}} \frac{n_{1r} e^{-\beta\epsilon_{n_1}} (1 - e^{\beta\hbar\omega_r}) \omega \Gamma_\omega(n_1)}{[\omega_r + \Delta_\omega(n_1) - \omega]^2 + \Gamma_\omega^2(n_1)}, \quad (15)$$

$$\alpha^{+-}(\omega) = 2\Lambda\mu_1^2 r_0^2 \left(\frac{x_0}{r_e}\right)^2 \times \sum_{n_1}^{n_{\max}-1} \frac{n_{1r}(n_{1x} + 1) e^{-\beta\epsilon_{n_1}} [1 - e^{\beta\hbar(\omega_r - \omega_x)}] \omega \Gamma_\omega(n_1)}{[\omega_r - \omega_x + \Delta_\omega(n_1) - \omega]^2 + \Gamma_\omega^2(n_1)}, \quad (16)$$

$$\alpha^{--}(\omega) = 2\Lambda\mu_1^2 r_0^2 \left(\frac{x_0}{r_e}\right)^2 \times \sum_{n_1}^{n_{\max}-1} \frac{n_{1r} n_{1x} e^{-\beta\epsilon_{n_1}} [1 - e^{\beta\hbar(\omega_r - \omega_x)}] \omega \Gamma_\omega(n_1)}{[\omega_r + \omega_x + \Delta_\omega(n_1) - \omega]^2 + \Gamma_\omega^2(n_1)}, \quad (17)$$

with  $n_1 \equiv (n_{1x}, n_{1y}, n_{1r})$  indexing the  $\epsilon_{n_1}$  states of the molecular Hamiltonian  $H_M$  and  $\beta = (k_B T)^{-1}$ . The functions  $\Delta_\omega(n_1)$  and  $\Gamma_\omega(n_1)$  are determined from the definition

$$B_\omega(n_1) \equiv -\Delta_\omega(n_1) - i\Gamma_\omega(n_1), \quad (18)$$

where the complex function  $B_\omega(n_1)$ , given in the Appendix, contains all the LPC effect on the absorption coefficient. In deriving Eqs. (14)–(17) we have further assumed that  $\omega_x = \omega_r \ll \omega_r$ .

The near IR spectrum profile is explicitly given by the components  $\alpha_N^-(\omega)$ ,  $\alpha^{+-}(\omega)$ , and  $\alpha^{--}(\omega)$ . The component  $\alpha_N^-(\omega)$  is a strong band centered near  $\omega_r$ , since it represents the pure vibrational transition  $\Delta J = 0, v = 0 \rightarrow v = 1$  of a free diatomic now perturbed by the LPC effect. The two combination components  $\alpha^{+-}(\omega)$  and  $\alpha^{--}(\omega)$  are weak bands centered near  $\omega_r - \omega_x$  and  $\omega_r + \omega_x$ , respectively. Each of these components, as shown by Eqs. (15)–(17), is a superposition of frequency and temperature dependent terms. Schematically,  $\alpha_N^-(\omega)$  contains as many terms as  $a_r^+$ -induced transitions from initial states  $n_2 = (n_{2x}, n_{2y}, 0)$  to final states  $n_1 = (n_{1x}, n_{1y}, 1)$  give a nonnegligible value. The band corresponds to the selection rule  $\Delta n_r = 1, \Delta n_\eta = 0$  ( $\eta = x, y$ ). Accordingly, the summations in  $\alpha^{+-}(\omega)$  and  $\alpha^{--}(\omega)$  arise from transitions induced by the operators  $a_\eta a_r^+, a_\eta^+ a_r^+$  that originate the selection rules  $\Delta n_r = 1, \Delta n_\eta = \pm 1$ . In this spectral region the functions  $\Delta_\omega(n_1)$  and  $\Gamma_\omega(n_1)$  vary slowly with frequency, consequently each term in the superposition is a Lorentzian-type function at a given temperature. The  $n$ th Lorentzian term in Eqs. (15)–(17) has a width  $\Gamma_\omega(n_1)$  and the unperturbed maxima  $\omega_r, \omega_r - \omega_x$ , or  $\omega_r + \omega_x$  are shifted by  $\Delta_\omega(n_1)$ . The origin of these shifts and widths are due to the LPC effect. Indeed, Eqs. (15)–(17) reduce to three delta functions when the LPC constants vanish. Closed expressions of  $\Delta_\omega(n_1), \Gamma_\omega(n_1)$  are obtained in the harmonic approximation, i.e., when only the second order LPC constants  $\lambda_{\eta b}^{(2)}$  are considered. If it is further assumed that  $\lambda_{xb}^{(2)} = \lambda_{yb}^{(2)} = \lambda_x/2$ , then the states  $n_1 = (n_{1x}, n_{1y}, 1)$  can be replaced by  $(n, 0, 1)$ ,<sup>14</sup> with  $n = 0, 1, \dots, n_{\max}$ . Thus, for the absorption case,

$$\Delta_\omega(n, 0, 1) = -\kappa \left[ (n+2) \gamma' \left( \frac{\omega_x + \Omega - \omega}{\omega_D} \right) + n \gamma' \left( \frac{-\omega_x + \Omega - \omega}{\omega_D} \right) \right],$$

$$\Gamma_\omega(n, 0, 1) = \pi \kappa \left[ (n+2) \gamma'' \left( \frac{\omega_x + \Omega - \omega}{\omega_D} \right) - n \gamma'' \left( \frac{-\omega_x + \Omega - \omega}{\omega_D} \right) \right]. \quad (19)$$

Here,  $\kappa = \pi(6\lambda_x)^2/\omega_D$ ,  $\Omega = \omega_r$  in  $\alpha_N^-(\omega)$ ,  $\Omega = \omega_r + \omega_x$  in  $\alpha^{--}(\omega)$ , and  $\Omega = \omega_r - \omega_x$  in  $\alpha^{+-}(\omega)$ . The functions  $\gamma'(\omega)$  and  $\gamma''(\omega)$  are defined in the Appendix and shown in Fig. 2 for two values of the temperature. In the  $\omega \sim \omega_r$  region, these functions vary slowly about the values of  $\gamma'(\pm \omega_x/\omega_D)$  and  $\gamma''(\pm \omega_x/\omega_D)$ , therefore leading to Lorentzian-type terms in the summations of Eqs. (15)–(17). The band profile of  $\alpha_N^-(\omega)$ ,  $\alpha^{+-}(\omega)$ ,  $\alpha^{--}(\omega)$  is given by the envelope of these Lorentzians. In general, the resulting band shape is not Lorentzian.

In the far IR there is only one component,  $\alpha_F^-(\omega)$ . The contributions to this band, centered near  $\omega_x$ , are a result of induced transitions such that  $\Delta n_r = 0, \Delta n_\eta = 1$  ( $\eta = x, y$ ). The functions  $\Delta_\omega(n_1)$  and  $\Gamma_\omega(n_1)$  in this case are not slowly varying with frequency and consequently the terms in the  $n_1$

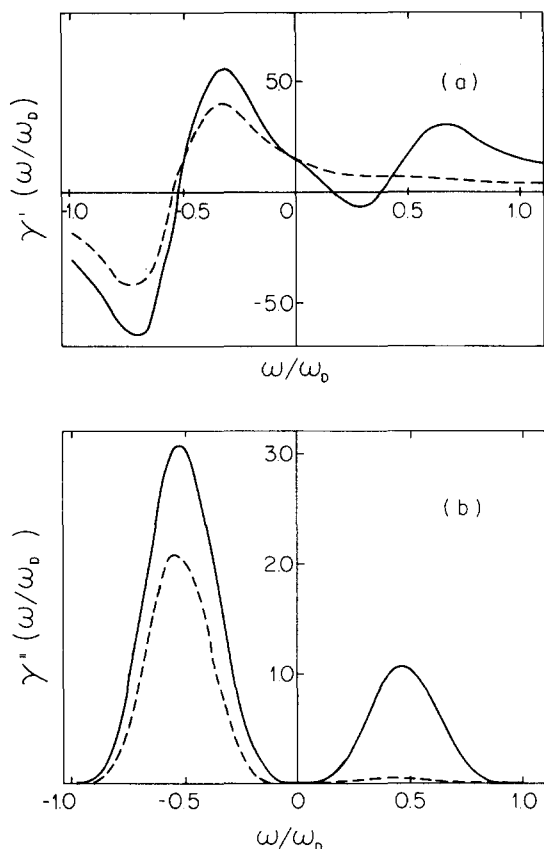


FIG. 2. Frequency dependence of (a)  $\gamma'$  function related to the shifts of the IR absorption bands [Eq. (A.7)] and (b)  $\gamma''$  function related to the broadening of the IR absorption bands [Eq. (A.8)], for  $T = 10$  K (dashed lines), and  $T = 40$  K (full lines), and  $\Theta_D = 85$  K.

summation are not Lorentzians. The harmonic approximation of the latter yields, for  $n_1 = (n, 0, 0)$ :

$$\begin{aligned} \Delta_\omega(n, 0, 0) &= \kappa \left[ (n-2) \gamma' \left( \frac{2\omega_x - \omega}{\omega_D} \right) \right. \\ &\quad \left. - n \gamma' \left( -\frac{\omega}{\omega_D} \right) \right], \\ \Gamma_\omega(n, 0, 0) &= -\pi \kappa \left[ (n-2) \gamma'' \left( \frac{2\omega_x - \omega}{\omega_D} \right) \right. \\ &\quad \left. - n \gamma'' \left( -\frac{\omega}{\omega_D} \right) \right]. \end{aligned} \quad (20)$$

Two such functions vary in the frequency region  $\omega \sim \omega_x$  as shown in Fig. 2. Therefore, the resulting expressions for the various  $n_1$  contributions to  $\alpha_F(\omega)$  have to be calculated considering explicitly the  $\omega$  dependence of  $\gamma'(\omega)$  and  $\gamma''(\omega)$ .

At low temperatures of about 10 K, two or three terms contribute to each of the four absorption coefficient components. At higher temperatures the number of nonnegligible terms increases and the peak position as well as the width of each term change. This effect is due to the temperature dependence of the  $\Delta_\omega(n_1)$  and  $\Gamma_\omega(n_1)$  functions. Eventually, at high enough temperatures, there will be nonvanishing contributions up to a maximum number  $n_{\max}$  such that the energy difference between the higher state  $\epsilon_{n_{\max}}$  and the initial state  $\epsilon_{n_2} \equiv \epsilon_0$  is of the order of  $V_0$ , the potential barrier to libration. As the energy difference is increased above this

value, the molecule rotates almost freely. Therefore, the  $n_1$  summations are finite, containing at most  $n_{\max}$  terms. At low temperatures, as is the case of interest for molecules trapped in matrices, very few terms give a nonvanishing contribution to these summations and the maximum value is seldom reached. Thus, the profile of each band is just a superposition of two or three functions (Lorentzian-type or not). In a preceding paper,<sup>14</sup> we gave the LPC result for liquids which yields a more complex envelope for each band, due to the larger number of contributing terms in the corresponding summations.

All together, Eqs. (14)–(17) give the LPC analytical expression for the absorption coefficient in the IR region. If now we compare such result to experimental data, the constants in the expression ( $\omega_x$ ,  $n_{\max}$ , and the LPC constants) will acquire values corresponding to the species under treatment. The number of LPC constants worthwhile to be included depends on the available experimental data. As we discuss in the next section, certain features of the experiment can be fitted to Eqs. (14)–(17) and from there one obtains numerical values of the unknown constants. The meaning of these unknown constants is very clear:  $\omega_x$  is the libration frequency,  $n_{\max}$  measures the barrier height to libration, and  $\lambda_{\eta b}^{(2)}$ ,  $\lambda_{\eta b b}^{(3)}$  provide the interaction between libration excitations and phonons. Whenever  $\omega_x$  has a small value, the  $n_{\max}$  terms in Eqs. (14)–(17) will be sharp and closely spaced giving a structured envelope. Larger values of  $\omega_x$  tend to smooth over the band profile. For fixed  $\omega_x$ , the widths and red shifts of the terms composing the central and high frequency bands increase with increasing  $\lambda$  values. One might be tempted to interpret the  $\Gamma_\omega(n_1)$  in the  $n_1$  summations giving rise to the three bands, as proportional to the inverse of as many relaxation times as significant terms are in the sums. If that is so, the librational relaxation will be governed by several fast processes with characteristic times which depend on temperature. In Fig. 2 it is shown that the functions used to calculate  $\Gamma_\omega(n_1)$  increase with increasing temperature. One should expect that these characteristic times decrease with increasing temperature. In what concerns the band shape, or a whole envelope of Lorentzians, at very low temperatures only red shifted bands about  $\omega_r$  are possible. When temperature is raised, the bands can shift towards the blue.

The emission process is similar, when viewed under this scope. When emission takes place, the libration–vibration band  $n_r = 1 \rightarrow n_r = 0$ ,  $\Delta n_x = 0$  is composed by final states  $n_1$  that give rise to functions  $\Delta_\omega(n, 0, 0)$ ,  $\Gamma_\omega(n, 0, 0)$ . These functions are equal to those given in Eq. (19), but the exponential factors in Eqs. (15)–(17) are very small. The overall result is that librational relaxation gives rise to linewidths both in absorption and emission. Vibrational energy relaxation due to phonons gives a negligible contribution<sup>10,17</sup> to the broadenings when compared to the LPC mechanism.

### III. COMPARISON TO EXPERIMENT AND DISCUSSION

Dubost<sup>1,13</sup> measured the near IR absorption spectra of CO trapped in Ne, Ar, Kr, and Xe matrices. The experiments were performed at various temperatures, 8 K being the lowest. The main features of the active monomeric spectra are very similar for the different rare-gas matrices, i.e., a

TABLE I. Calculated and experimental (Ref. 1) absorption frequencies, line shifts, and linewidths (in  $\text{cm}^{-1}$ ) for CO in rare gas matrices.

	Ne	Ar	Kr	Xe	Assignment
<b>Strong bands</b>					
experiment <sup>a</sup> ( $\nu_{\text{exp}}$ )	2140.9	2138.6	2135.7	2133.2	$\nu_{0 \rightarrow 1}$
$\nu_{\text{theor}} = \nu_r + \Delta\nu_{\omega}(0,0,1)$	2143.3	2140.2	2141.7	2142.7	$\Delta n_r = 1, \Delta n_x = 0$
<b>Shift</b>					
$\nu_{\text{theor}} - \nu_r$	-0.2	-3.3	-2.8	-0.8	
<b>Linewidth</b>					
experiment <sup>a</sup>	0.16	0.47	0.55	0.55	
this work	0.14	0.46	0.54	0.55	
<b>Weak bands</b>					
experiment <sup>a</sup>	2156.7	2150.0	2146.0	2143.0	$\nu_{0 \rightarrow 1}$
$\nu_r + \nu_x + \Delta\nu_{\omega}(1,0,1)$	2159.1	2151.3	2151.7	2152.5	
$\bar{\nu}_r + \nu_x + \Delta\nu_{\omega}(1,0,1)$	2156.7	2146.4	2143.9	2142.2	$\Delta n_r = 1, \Delta n_x = 1$
<b>Shift</b>					
$\nu_{\text{theor}} - (\nu_r + \nu_x)$	-16.9	-19.5	-15.7	-13.2	
$\nu_{\text{theor}} - (\bar{\nu}_r + \nu_x)$	-14.5	-17.9	-10.7	-3.7	
<b>Linewidth</b>					
this work	1.3	1.0	1.3	2.0	

<sup>a</sup>) Reference 1.

central band with two shoulders towards the high and low frequency regions. The central peak at  $\nu_{\text{exp}}$  is red shifted with respect to the  $\nu = 0 \rightarrow \nu = 1$ ,  $\Delta J = 0$  transition in gaseous CO. This peak, as well as the shoulders, grow wider and less intense with increasing temperature. In fact, the low frequency shoulder is only detected when temperature is raised.

Three features of near IR absorption data are fitted according to Eqs. (15)–(17): the relative position and relative intensity of the  $\Delta n_r = 1$ ,  $\Delta n_x = 1$  and  $\Delta n_r = 1$ ,  $\Delta n_x = 0$  peaks and the central band linewidth. The values of the constants involved in the theory are obtained from one fit to the spectrum at the lowest available experimental temperature and molecular concentration. Since the LPC model does not include inhomogeneous broadening, the fitted LPC constants may be overestimated. That is so because the experimental absorption linewidth contains some inhomogeneous broadening<sup>17</sup> which has not been taken in consideration. The comparison to experiment is therefore subject to this qualification.

In what follows we consider the harmonic approximation of Eqs. (14)–(17) and give all frequencies as  $\nu = \omega/2\pi$ . Numerical values of three unknowns, the LPC  $\lambda_x$ ,  $\omega_x$ , and  $n_{\text{max}}$  are to be extracted from comparison to experiments of CO trapped in rare-gas matrices. All other constants have the values of unperturbed systems: (i) the gaseous CO spectroscopic constants  $\nu_r \equiv \nu_{0 \rightarrow 1} = 2143.5 \text{ cm}^{-1}$ ,  $r_e = 1.128 \text{ \AA}$ , and  $m_{\text{AB}} = 6.86^{18}$ ; (ii) the rare-gas Debye temperature of the solid at low temperatures, 63, 85, 73, and 55 K for Ne, Ar, Kr, and Xe, respectively.<sup>19</sup>

The level of agreement shown in Table I between experiment and theory is achieved with the values of the constants given in Table II. In Table I, the shift of the strong bands is defined as the frequency difference between the calculated (or experimental) peak maximum of the envelope  $\nu_{\text{theor}}$  (or  $\nu_{\text{exp}}$ ) and the gas value of the vibrational frequency  $\nu_r$ , i.e.,  $\nu_{\text{theor}} - \nu_r$  or  $\nu_{\text{exp}} - \nu_r$ . The shift of the weak bands

defined as  $\nu_{\text{theor}} - (\nu_r - \nu_x)$  is also shown in Table I. The linewidth is measured both theoretically and experimentally as the full width at half-maximum of the hole band. As it is clear from the values of the strong bands position, the LPC model only gives part of the shift. This is to be expected, since the coupling is too weak to produce intramolecular changes due to the molecule neighboring surroundings such as large anharmonicities. Therefore, in order to obtain a better comparison, we define an effective unperturbed vibrational frequency  $\bar{\nu}_r$ :

$$\bar{\nu}_r = \nu_{\text{exp}} + (\nu_r - \nu_{\text{theor}}), \quad (21)$$

such that the maximum of the theoretical strong band extracted from Eq. (15) coincide with the experimental peak  $\nu_{\text{exp}}$ . The values of  $\bar{\nu}_r$  are reported in Table II. The whole spectrum profile is recalculated with  $\bar{\nu}_r$ , as displayed in Fig. 3 for CO in Ne, Ar, Kr, and Xe matrices. The  $\nu$  scale in this figure is measured with respect to the  $\nu_{\text{exp}}$  given in Table I. The calculated shifts and widths obtained using  $\bar{\nu}_r$ , instead of  $\nu_r$ , do not differ from those reported in Table I, whereas the calculated weak bands maxima do change as indicated in the same table. The LPC effect is clear in the four matrices. The tendency with increasing mass of the host atoms is to shrink the spectral structure into one central peak by lowering  $\omega_x$  and broadening the side bands. The broadening is a result of considering each band as a superposition of  $n_{\text{max}}$  Lorent-

TABLE II. Numerical values of the constants in Eqs. (14)–(17) obtained from the fit to CO-rare gas matrices experiments at 8 K.

	Ne	Ar	Kr	Xe
$\omega_x (\text{cm}^{-1})$	16.7	16.2	13.9	12.4
$\lambda_x (\text{cm}^{-1})$	0.6	2.4	1.8	1.0
$n_{\text{max}}$	4	4	4	4
$V_0 (\text{cm}^{-1})$	75.2	72.9	62.6	55.8
$\bar{\nu}_r (\text{cm}^{-1})$	2141.1	2141.9	2138.5	2134.0

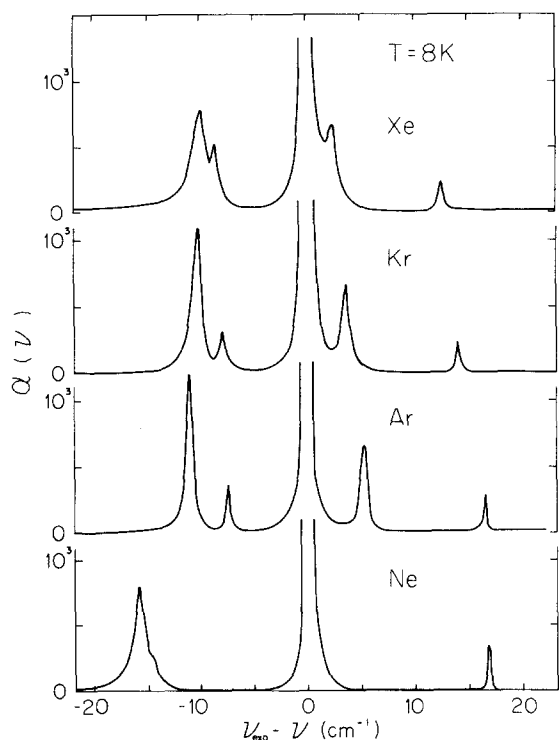


FIG. 3. Near IR absorption spectra for CO trapped in rare-gas matrices at 8 K calculated from Eqs. (15)–(17) using the constants cast in Table II.  $\alpha(\nu)$  is given in arbitrary units and the  $\nu$  scale is referred to the experimental value of  $\nu_{0-1}$  given in Table I.

zian-type functions of width given by  $\Gamma_{\omega}(n,0,1)$ . In fact, the central band is resolved into one unique envelope for Xe.

Once the values of the constants are fixed we change the temperature and show this effect in Fig. 4 for CO in an argon matrix. As the temperature rises in the system, the bands are broader and the relative intensity of the central to side peak decreases. At  $T = 36$  K, the spectral structure has almost

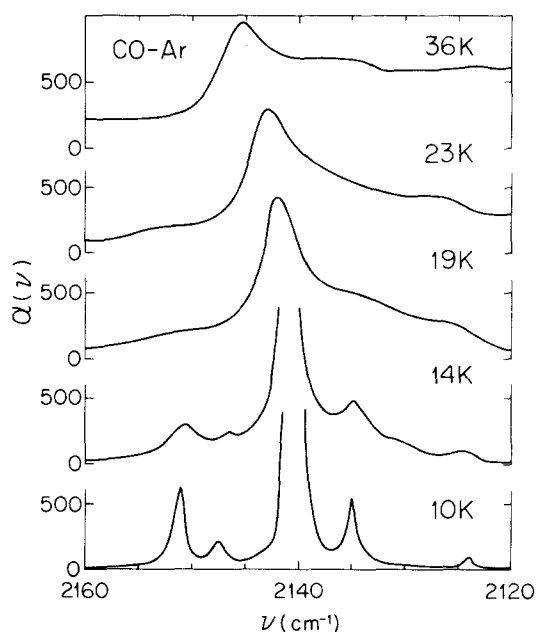


FIG. 4. Calculated temperature dependence of the near IR absorption spectrum for CO trapped in an argon matrix.  $\alpha(\nu)$  is given in arbitrary units.

disappeared, being substituted by a broad feature. During the heating process, the number of terms in each component were controlled to be  $n_{\max}$ , but the weight of these terms increases considerably, yielding increasing blue shifts and drastic shape changes especially in the low frequency side of the central band.

It is instructive to quantitatively compare our approach with experiments, since the procedure allows to extract values for the constants in the theoretical results. Such constants may further be used to gain insight into other spectral properties. The unperturbed frequencies  $\omega_x$  in Table II are of the order of Dubost's<sup>1,13</sup> assignments for a pure libration transition. The latter decreased with increasing mass of the host atoms, same as the calculated  $\omega_x$ . The LPC constants obtained in this work are small, confirming the hypothesis that this effect is indeed a small perturbation. Despite the small values of the strength, the LPC effect is enough to produce linewidths successfully in agreement with Dubost's experiment (see Table I and Fig. 3). The LPC effect is also the sole interaction that gives the band temperature dependence, reproducing correctly the experimental results for CO–Ar (Fig. 4). Inspection of the  $\lambda_x$  values in Table II shows that except for CO–Ne, the decreasing ordering parallels that of the librational frequencies. The manifestation of an anomaly for Ne is also evident in the sequence of rare-gas Debye temperatures. Finally, the libration barriers obtained in this work are in good agreement with those reported in the literature.<sup>1</sup>

From the above results we can predict the dipolar contribution of CO to the absorption coefficient in the far IR. Thus, taking the values of the constants in Eq. (14) as those given in Table II, we are able to determine the absorption profile as shown in Fig. 5 for CO–Ar. That is, identical input

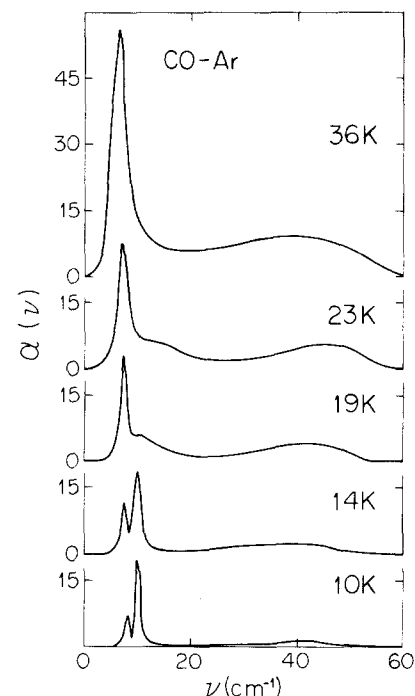


FIG. 5. Temperature dependence of the dipolar contribution to the far IR absorption spectrum for CO trapped in an argon matrix calculated from Eq. (14) and using the constants collected in Table II.

information produces the bands and temperature variation as depicted in the figure. The LPC effect, even in its harmonic approximation, gives a very strong temperature dependence of the spectral lines. This is a new effect and an improvement with respect to the predictions we gave in the 1D case.<sup>2</sup> When  $\alpha_{\bar{F}}(\omega)$  is compared to the calculated far IR spectra of CO in liquid Ar,<sup>14</sup> we can see the drastic changes due to temperature and to the environment. CO in a matrix produces a rather strong and localized band near the unperturbed  $\omega_x$  librational frequency. The same molecule in liquid argon gives rise to a broad and extremely blue shifted band with respect to  $\omega_x$ , even though the value of the LPC constant  $\lambda_x$  is of the same order in both cases, i.e., equals  $1.8 \text{ cm}^{-1}$  in the liquid and  $2.4 \text{ cm}^{-1}$  in the solid.

As the title of this paper conveys, only one aspect of the LPC theory for molecules in solid matrices has been discussed. The results of this theoretical study, when compared to experiments of CO trapped in a number of solid matrices, yield quantitative agreement and seem to indicate that the LPC model does indeed take account of the main interactions responsible for the line shape temperature dependence. The near as well as far IR components are given by Eqs. (14)–(17). These components are envelopes of several weighted functions with peaks and widths depending on the LPC strength as well as on temperature. The analytical expressions that we provide for the absorption coefficient  $\alpha(\omega)$  contain three unknowns,  $\omega_x$ ,  $\lambda_x$ , and  $n_{\text{max}}$  (or  $V_0$ ); values for all three can be extracted from a fit to experiment. Furthermore, all three quantities have a very precise meaning, i.e.,  $\omega_x$  and  $V_0$  are the librational frequency and height of the static potential and  $\lambda_x$  is the harmonic LPC constant. Further far IR experiments of molecules with high orientational sensitivity should lead to greater understanding of these systems, since they should allow to compare with the LPC theory in its complete version.

## ACKNOWLEDGMENTS

We are grateful to Professor Shigeji Fujita for valuable discussions on the use of the connected diagram method, and

to Dr. P. A. Mello and Dr. E. Martina for interesting comments. We acknowledge J. del Moral for calculations in the early stages of this work and Dr. E. Poulain for help with the drawings. EBB acknowledges the Fulbright and AAUW Foundations for a research award.

## APPENDIX

The constants  $f_{\eta}^{\sigma}$  and  $f_{\eta}^{\sigma\sigma'}$  in Eq. (9) for  $\eta = x, y$  and  $\sigma = l, t_1, t_2$  obtained from Fig. 1 can be written as

$$f_x^l = \sin \theta_p \cos \varphi_p; \quad f_x^{t_1} = \cos \varphi_p; \quad f_x^{t_2} = \cos \theta_p \cos \varphi_p;$$

$$f_y^l = \sin \theta_p \sin \varphi_p; \quad f_y^{t_1} = \sin \varphi_p; \quad f_y^{t_2} = \cos \theta_p \sin \varphi_p;$$

$$f_{\eta}^{\sigma\sigma'} = f_{\eta}^{\sigma} \delta_{\sigma\sigma'} \quad (\text{A1})$$

with  $\delta_{\sigma\sigma'}$  being a Kronecker delta.

The constants in Eq. (11) for  $\eta = x, y$  are given by

$$m_{\eta}^{+} = m_{\eta}^{-} = \mu_0 \frac{\eta_0}{r_e},$$

$$m_{\eta}^{++} = m_{\eta}^{+-} = m_{\eta}^{-+} = m_{\eta}^{--} = \mu_1 r_0 \frac{\eta_0}{r_e}, \quad (\text{A2})$$

where  $\eta_0 = (\hbar/2m_{\text{AB}}\omega_{\eta})^{1/2}$  and  $r_0 = \hbar/2m_{\text{AB}}\omega_r)^{1/2}$ . When  $\eta = z$ ,

$$m_z^{+} = m_z^{-} = \mu_1 r_0,$$

$$m_z^{++} = m_z^{+-} = m_z^{-+} = m_z^{--} = 0. \quad (\text{A3})$$

The expression for the  $B_{\omega}(n_1) \equiv -\Delta_{\omega}(n_1) - i\Gamma_{\omega}(n_1)$  function responsible of the LPC shifts and broadenings is given by

$$B_{\omega}(n_1) = B_{\omega}^{(1)}(n_1) + B_{\omega}^{(2)}(n_1), \quad (\text{A4})$$

where  $B_{\omega}^{(1)}(n_1)$  and  $B_{\omega}^{(2)}(n_1)$  are associated to one and two phonons processes, respectively. These are given by

$$\begin{aligned} B_{\omega}^{(1)}(n_1) = & \sum_{\eta=x,y} \sum_{s=1}^3 (\lambda_{\eta b}^s)^2 \sum_{\mathbf{k}\sigma} \sum_{n_3} (1 + n_{\mathbf{k}\sigma}) \left\{ (\gamma_{\mathbf{k}}^s)_{13} [(\gamma_{\mathbf{k}}^s)_{31}^{+} - A_{31,12}(\gamma_{\mathbf{k}}^s)_{12}^{+}] \frac{1}{\epsilon_{32} + \omega_{\mathbf{k}\sigma} - \omega + ia} \right. \\ & \left. + (\gamma_{\mathbf{k}}^s)_{12}^{+} [(\gamma_{\mathbf{k}}^s)_{21} - A_{31,12}(\gamma_{\mathbf{k}}^s)_{13}] \frac{1}{\epsilon_{11} - \omega_{\mathbf{k}\sigma} - \omega + ia} \right\} \\ & + \sum_{\eta=x,y} \sum_{s=1}^3 (\lambda_{\eta b}^s)^2 \sum_{\mathbf{k}\sigma} \sum_{n_3} n_{\mathbf{k}\sigma} \left\{ (\gamma_{\mathbf{k}}^s)_{13} [(\gamma_{\mathbf{k}}^s)_{31}^{+} - A_{31,12}(\gamma_{\mathbf{k}}^s)_{12}^{+}] \frac{1}{\epsilon_{32} - \omega_{\mathbf{k}\sigma} - \omega + ia} \right. \\ & \left. + (\gamma_{\mathbf{k}}^s)_{12}^{+} [(\gamma_{\mathbf{k}}^s)_{21} - A_{31,12}(\gamma_{\mathbf{k}}^s)_{13}] \frac{1}{\epsilon_{11} + \omega_{\mathbf{k}\sigma} - \omega + ia} \right\} \quad (\text{A5}) \end{aligned}$$

with  $A_{31,12} = (A_{\eta})_{31}/(A_{\eta})_{12}$ ,  $A_{\eta}$  is either  $a_{\eta}^{+}$ ,  $a_{\eta}^{-}$ ,  $a_{\eta}^{+}a_{\eta}^{-}$  or  $a_{\eta}^{-}a_{\eta}^{+}$ . The subindexes 1,2,3 indicate the states  $n_1, n_2, n_3$ ,  $\gamma_{\mathbf{k}}^s = (\omega_{\text{D}}/\omega_{\mathbf{k}\sigma})^{1/2} F_{\eta}(\mathbf{k}\sigma)(a_{\eta}^{+} + a_{\eta}^{-})^s$  and  $n_{\mathbf{k}\sigma} = (e^{\beta\hbar\omega_{\mathbf{k}\sigma}} - 1)^{-1}$ .

$$\begin{aligned}
B_{\omega}^{(2)}(n_1) = & \sum_{\eta=x,y} \sum_{s=1}^2 (\lambda_{\eta bb}^s)^2 \sum_{\mathbf{k}\sigma} \sum_{n_3} (1+n_{\mathbf{k}\sigma})(1+n_{\mathbf{k}'\sigma'}) \left\{ (\gamma_{\mathbf{k}\mathbf{k}'}^s)_{13} [(\gamma_{\mathbf{k}\mathbf{k}'}^s)_{31}^+ - A_{31,12}(\gamma_{\mathbf{k}\mathbf{k}'}^s)_{12}^+] \frac{1}{\epsilon_{32} + \omega_{\mathbf{k}\sigma} + \omega_{\mathbf{k}'\sigma'} - \omega + ia} \right. \\
& + (\gamma_{\mathbf{k}\mathbf{k}'}^s)_{12}^+ [(\gamma_{\mathbf{k}\mathbf{k}'}^s)_{21} - A_{31,12}(\gamma_{\mathbf{k}\mathbf{k}'}^s)_{13}] \frac{1}{\epsilon_{11} + \omega_{\mathbf{k}\sigma} - \omega_{\mathbf{k}'\sigma'} - \omega + ia} \left. \right\} \\
& + \sum_{\eta=x,y} \sum_{s=1}^2 (\lambda_{\eta bb}^s)^2 \sum_{\mathbf{k}\sigma} \sum_{n_3} n_{\mathbf{k}\sigma} n_{\mathbf{k}'\sigma'} \left\{ (\gamma_{\mathbf{k}\mathbf{k}'}^s)_{13} [(\gamma_{\mathbf{k}\mathbf{k}'}^s)_{31}^+ - A_{31,12}(\gamma_{\mathbf{k}\mathbf{k}'}^s)_{12}^+] \frac{1}{\epsilon_{32} - \omega_{\mathbf{k}\sigma} - \omega_{\mathbf{k}'\sigma'} - \omega + ia} \right. \\
& + (\gamma_{\mathbf{k}\mathbf{k}'}^s)_{12}^+ [(\gamma_{\mathbf{k}\mathbf{k}'}^s)_{21} - A_{31,12}(\gamma_{\mathbf{k}\mathbf{k}'}^s)_{13}] \frac{1}{\epsilon_{11} + \omega_{\mathbf{k}\sigma} + \omega_{\mathbf{k}'\sigma'} - \omega + ia} \left. \right\} \\
& + \sum_{\eta=x,y} \sum_{s=1}^2 (\lambda_{\eta bb}^s)^2 \sum_{\mathbf{k}\sigma} \sum_{n_3} n_{\mathbf{k}\sigma} (1+n_{\mathbf{k}'\sigma'}) \left\{ (\gamma_{\mathbf{k}\mathbf{k}'}^s)_{13} [(\gamma_{\mathbf{k}\mathbf{k}'}^s)_{31}^+ - A_{31,12}(\gamma_{\mathbf{k}\mathbf{k}'}^s)_{12}^+] \frac{1}{\epsilon_{32} + \omega_{\mathbf{k}\sigma} - \omega_{\mathbf{k}'\sigma'} - \omega + ia} \right. \\
& + (\gamma_{\mathbf{k}\mathbf{k}'}^s)_{12}^+ [(\gamma_{\mathbf{k}\mathbf{k}'}^s)_{21} - A_{31,12}(\gamma_{\mathbf{k}\mathbf{k}'}^s)_{13}] \frac{1}{\epsilon_{11} - \omega_{\mathbf{k}\sigma} + \omega_{\mathbf{k}'\sigma'} - \omega + ia} \left. \right\} \\
& + \sum_{\eta=x,y} \sum_{s=1}^2 (\lambda_{\eta bb}^s)^2 \sum_{\mathbf{k}\sigma} \sum_{n_3} (1+n_{\mathbf{k}\sigma}) n_{\mathbf{k}'\sigma'} \left\{ (\gamma_{\mathbf{k}\mathbf{k}'}^s)_{13} [(\gamma_{\mathbf{k}\mathbf{k}'}^s)_{31}^+ - A_{31,12}(\gamma_{\mathbf{k}\mathbf{k}'}^s)_{12}^+] \frac{1}{\epsilon_{32} - \omega_{\mathbf{k}\sigma} + \omega_{\mathbf{k}'\sigma'} - \omega + ia} \right. \\
& + (\gamma_{\mathbf{k}\mathbf{k}'}^s)_{12}^+ [(\gamma_{\mathbf{k}\mathbf{k}'}^s)_{21} - A_{31,12}(\gamma_{\mathbf{k}\mathbf{k}'}^s)_{13}] \frac{1}{\epsilon_{11} + \omega_{\mathbf{k}\sigma} - \omega_{\mathbf{k}'\sigma'} - \omega + ia} \left. \right\}. \tag{A6}
\end{aligned}$$

Here

$$\gamma_{\mathbf{k}\mathbf{k}'}^s = \frac{\omega_D}{(\omega_{\mathbf{k}\sigma} \omega_{\mathbf{k}'\sigma'})^{1/2}} F_{\eta}(\mathbf{k}\sigma, \mathbf{k}'\sigma') (a_{\eta}^+ + a_{\eta})^s.$$

The functions  $\gamma'(\omega/\omega_D)$  and  $\gamma''(\omega/\omega_D)$  are defined as

$$\gamma' \left( \frac{\omega}{\omega_D} \right) = \int_{-1}^1 \frac{t \cos(2\pi t - 1)^2}{\omega/\omega_D - t} [\exp(\Theta_D t / T) - 1]^{-1} dt, \tag{A7}$$

$$\gamma'' \left( \frac{\omega}{\omega_D} \right) = \frac{\omega}{\omega_D} [\cos(2\pi\omega/\omega_D) - 1]^2 [\exp(\Theta_D \omega/\omega_D T) - 1]^{-1}, \tag{A8}$$

where  $\Theta_D$  is the crystal Debye's temperature and  $T$  is the absolute temperature.

<sup>1</sup>H. Dubost, Chem. Phys. **12**, 139 (1976).

<sup>2</sup>E. Blaisten-Barojas and M. Allavena, J. Phys. C **9**, 3121 (1976).

<sup>3</sup>L. Pauling, Phys. Rev. **36**, 430 (1930).

<sup>4</sup>A. F. Devonshire, Proc. R. Soc. London Ser. A. **153**, 601 (1936).

<sup>5</sup>J. Manz, J. Am. Chem. Soc. **102**, 1801 (1980).

<sup>6</sup>H. Friedmann and S. Kimel, J. Chem. Phys. **43**, 3925 (1965).

<sup>7</sup>H. Friedmann and S. Kimel, J. Chem. Phys. **47**, 3589 (1967).

<sup>8</sup>P. O. Mannheim and H. Friedmann, Phys. Status Solidi **39**, 409 (1970).

<sup>9</sup>A. Nitzan, S. Mukamel, and J. Jortner, J. Chem. Phys. **63**, 200 (1975).

<sup>10</sup>E. Blaisten-Barojas and M. Allavena, Int. J. Quantum Chem. **7**, 195 (1973).

<sup>11</sup>F. Mauricio, S. Velasco, C. Girardet, and L. Galatry, J. Chem. Phys. **76**, 1624 (1982).

<sup>12</sup>M. Allavena, H. Chakroun, and D. White, J. Chem. Phys. **77**, 1757 (1982).

<sup>13</sup>H. Dubost, A. Lecuyer, and R. Charneau, Chem. Phys. Lett. **66**, 191 (1979).

<sup>14</sup>I. L. Garzón, E. Blaisten-Barojas, and S. Fujita, J. Chem. Phys. **82**, 1772 (1985).

<sup>15</sup>S. Fujita *Introduction to Non-Equilibrium Quantum Statistical Mechanics* (Saunders, Philadelphia, 1966), Chaps. 5 and 7.

<sup>16</sup>A. Lodder and S. Fujita, J. Phys. Soc. Jpn. **25**, 774 (1968).

<sup>17</sup>H. Dubost, *Inert Gases, Potential, Dynamics and Energy Transfer in Doped Crystals*, edited by M. L. Klein (Springer, New York, 1984), p. 145.

<sup>18</sup>G. Herzberg, *Spectra of Diatomic Molecules* (van Nostrand, New York, 1959), p. 521.

<sup>19</sup>N. N. Aschroft and N. D. Mermin, *Solid State Physics* (Holt, Rinehart, and Winston, New York, 1976).